Nanoscale

PAPER

View Article Online
View Journal | View Issue

Cite this: *Nanoscale*, 2021, **13**, 9706

Super resolution microscopy reveals DHA-dependent alterations in glioblastoma membrane remodelling and cell migration†

Xia Xu,‡ Yixiong Wang,‡ Won-Shik Choi, Xuejun Sun and Roseline Godbout *

Brain fatty acid binding protein (FABP7; B-FABP) promotes glioblastoma (GBM) cell migration and is associated with tumor infiltration, properties associated with a poor prognosis in GBM patients. FABP7-expressing neural stem-like cells are known to drive tumor migration/infiltration and resistance to treatment. We have previously shown that FABP7's effects on cell migration can be reversed when GBM cells are cultured in medium supplemented with the omega-3 fatty acid, docosahexaenoic acid (DHA). Here, we use super-resolution imaging on patient-derived GBM stem-like cells to examine the importance of FABP7 and its fatty acid ligands in mitigating GBM cell migration. As FABPs are involved in fatty acid transport from membrane to cytosol, we focus on the effect of FABP7 and its ligand DHA on GBM membrane remodeling, as well as FABP7 nanoscale domain formation on GBM membrane. Using quantitative plasma membrane lipid order imaging, we show that FABP7 expression in GBM cells correlates with increased membrane lipid order, with DHA dramatically decreasing lipid order. Using super-resolution stimulated emission depletion (STED) microscopy, we observe non-uniform distribution of FABP7 on the surface of GBM cells, with FABP7 forming punctate nanoscale domains of ~100 nm in diameter. These nanodomains are particularly enriched at the migrating front of GBM cells. Interestingly, FABP7 nanodomains are disrupted when GBM cells are cultured in DHA-supplemented medium. We demonstrate a tight link between cell migration, a higher membrane lipid order and increased FABP7 nanoscale domains. We propose that DHA-mediated disruption of membrane lipid order and FABP7 nanodomains forms the basis of FABP7/DHA-mediated inhibition of cell migration in GBM.

Received 5th April 2021,
Accepted 15th May 2021

DOI: 10.1039/d1nr02128a

rsc.li/nanoscale

Introduction

GBM is the most common and malignant primary brain cancer. Despite aggressive treatment and extensive research, GBM remains one of the most deadly cancers, with the majority of patients dying within 15 months of their diagnosis.[1] The highly infiltrative/invasive properties of GBM and treatment-resistant cancer stem cells are believed to be responsible for the high recurrence rates observed after radiation treatment and chemotherapy.[2] Brain fatty acid binding protein (B-FABP or FABP7) is normally expressed in neural stem cells during development.[3,4] FABP7 is also expressed in GBM stem-like cells and is preferentially found at the infiltrative edges of GBM tumors.[5–7] FABP7, whose preferred ligands are polyunsaturated fatty acids (PUFAs), has previously been shown to localize to the nucleus of GBM cells where its expression is associated with epidermal growth factor receptor (EGFR)[8] and the transfer of PUFAs to transcription factors such as peroxisome proliferator associated receptors (PPARs).[9] However, FABP7 is also found in the cytoplasm and plasma membrane of GBM cells.[5,10]

The main components of the plasma membrane are phospholipids.[11] The plasma membrane order refers to physical phase segregation of phospholipid bilayers, with the liquid-ordered (Lo) phase co-existing with the liquid-disordered (Ld) phase.[12] The ordered lipid domain (Lo phase), also referred to as tightly packed membrane nanodomains, is characterized by clustering of membrane proteins and lipids, including sphingolipids, cholesterol and saturated phospholipids. However, the presence of unsaturated phospholipids impairs lipid packing, resulting in a lower state of lipid order (Ld phase).[12] In addition to lipid composition, plasma membrane order is also determined by actin cytoskeletal activity.[13] GBM cell migration is accompanied by protrusion and retraction of cell membranes, processes that require cytoskeleton remodelling.[14] Interestingly, FABP7 co-localizes with actin at the edge of

Cross Cancer Institute, University of Alberta, Department of Oncology, 11560 University Avenue, Edmonton, Alberta, Canada. E-mail: rgodbout@ualberta.ca

†Electronic supplementary information (ESI) available. See DOI: 10.1039/d1nr02128a

‡Equal contribution.

lamellipodial protrusions in FABP7-expressing GBM cells.[5] These results, combined with the fact that polyunsaturated fatty acids (PUFAs) are the preferred ligands of FABP7, suggest that FABP7's role in promoting GBM cell migration is related to plasma membrane order. Relevant to our study, Laurdan (6-dodecanoyl-2-dimethylaminonaphthalene), a lipid phase sensitive fluorescent probe,[15] reveals increased plasma membrane order resulting from increased lipid saturation in GBM cells.[16]

Lipid-mediated protein membrane nanodomain formation is responsible for alterations in plasma membrane lipid order.[13] However, the mechanism behind these changes remained poorly understood until the emergence of super-resolution microscopy. Super-resolution microscopy, including direct stochastic optical reconstruction microscopy (dSTORM), photoactivated localization microscopy (PALM)[17] and stimulated emission depletion microscopy (STED), have allowed visualization and quantification of membrane protein distribution in the nanoscale.[18] In recent years, several membrane lipid-anchored proteins have been reported to form nanoscale domains, including PKCα, Ras and Rac1, which play essential roles in membrane protein-initiated signalling pathways (*i.e.*, Ca^{2+}-dependent signalling, Ras-driven proliferation pathway and Rac1 cell migration pathway, respectively).[19–21] As super-resolution microscopy overcomes the limitation of conventional optical microscopes, it allows direct visualization of membrane-anchored cytoskeletal protein nanodomains which is essential to our understanding of the mechanism underlying cell migration.[21,22]

Similar to brain, GBM tumors are rich in PUFAs, including ω-6 arachidonic acid (AA) and ω-3 docosahexaenoic acid (DHA).[23] As both AA and DHA are highly hydrophobic molecules, their transport within GBM cells relies on fatty acid transport proteins, such as FABP7.[24] DHA, a preferred ligand of FABP7, attenuates KRas-driven proliferation in colon cancer cells by altering KRas protein membrane nanodomain formation.[25] FABPs have been shown to increase the uptake of fatty acids from the cellular microenvironment.[26] FABP7's affinity for DHA and AA,[27,28] combined with its localization at the plasma membrane, cytoplasm and nucleus,[5,10] suggest a role for FABP7 in both the uptake of DHA and AA from the microenvironment and its subsequent intracellular distribution. In agreement with this, using Nuclear Magnetic Resonance (NMR) and Electron Spin Resonance (ESR), FABP7 was found to undergo a conformational alteration upon binding to fatty acid ligands, resulting in its dissociation from biomimetic model membranes.[29,30] Our previous work has shown that DHA inhibits GBM cell migration in a FABP7-dependent manner.[10] With its 6 unsaturated bonds and very long carbon chain,[31] DHA's inhibitory effect on GBM cell migration may be a direct consequence of its increased FABP7-dependent uptake and incorporation into plasma membrane phospholipids, thereby altering plasma membrane lipid order.

In this study, we use quantitative plasma membrane lipid order imaging to demonstrate an association between FABP7 expression in GBM cells and the formation of highly ordered plasma membrane lipid domains. We further show that increased plasma membrane lipid order correlates with increased GBM cell migration. DHA supplementation in culture medium has a dramatic effect on the plasma membrane lipid order of FABP7-expressing, but not non-FABP7-expressing, GBM cells. FABP7 imaging using super-resolution microscopy indicates that FABP7 forms nanodomains on the membranes of both established GBM cell lines and patient-derived GBM stem-like cells. DHA supplementation inhibits cell migration and disrupts these FABP7 nanodomains. This is in contrast to AA and saturated stearic acid (SA) which have no effect on FABP7 nanodomains. Our results suggest that DHA inhibits GBM cell migration by decreasing membrane lipid order and disrupting FABP7 nanodomains.

Results

FABP7 expression increases GBM cell membrane lipid order

We have previously reported correlation between FABP7 expression and increased migration in GBM cells.[5] Others have shown that the leading edge of migrating cells has high membrane order regions based on quantitative membrane lipid order analysis.[32,33] To examine the lipid packing state, an indication of hydration level, in GBM cell membrane phospholipids, we used the Laurdan dye. Ratiometrically measured alterations in membrane-bound Laurdan dye intensity at two different spectral channels (liquid-ordered (Lo) channel and liquid-disordered (Ld channel)), represented by the generalized polarization (GP) value, was used to quantitate plasma membrane lipid order.[15] We first examined the effect of FABP7 expression on GBM membrane lipid order. For these experiments, we used our previously described U87 stable transfectants[5] (U87-Control and U87-FABP7 cell lines) (Fig. 1a). The GP distribution obtained for each cell line is represented as pseudo-colored images, normalized histograms and average GP index values. Our results show that U87-FABP7 cells have a higher plasma membrane order (right shifting of GP histograms and higher GP index values) compared to U87-Control cells (Fig. 1b–d). These results indicate that FABP7 expression promotes highly ordered/rigid plasma membrane formation in GBM cells.

We also carried out Laurdan experiments with U251 control cells (U251-shControl) which naturally express FABP7 and U251 cells depleted of FABP7 using lentiviral shRNA constructs (U251-shFABP7) (Fig. 1a). Consistent with our U87 data, FABP7-depleted U251 cells (U251-shFABP7-2) have a lower plasma membrane order (left shifting of GP histograms and lower GP index values) compared to U251-Control cells (Fig. 1b–d). No significant effect was observed with U251-shFABP7-1, in keeping with the lower FABP7 knockdown efficiency observed in these cells.

Patient derived GBM cells cultured under conditions that promote the growth of cells with neural-stem like properties express high levels of FABP7.[7] When we repeated our Laurdan experiments with FABP7-expressing patient-derived ED501N

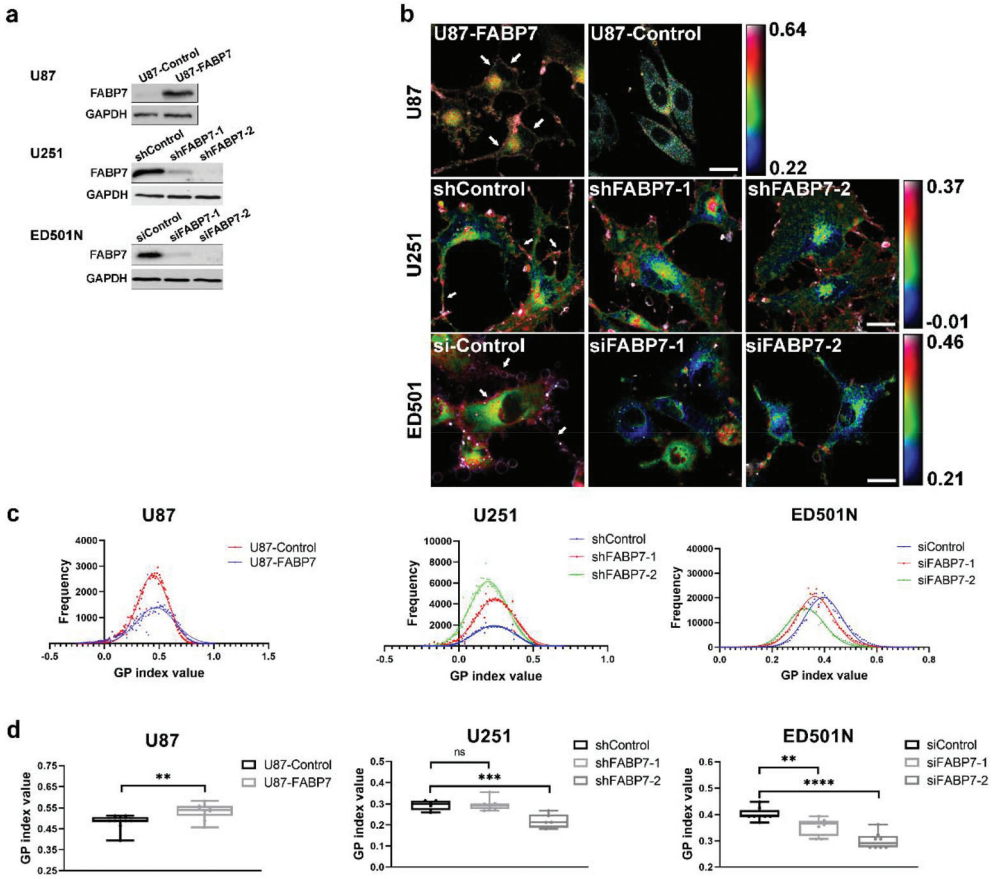

Fig. 1 FABP7 increases membrane lipid order in GBM cells and neurosphere cultures. (a) Western blot analysis showing FABP7 expression in stable U87-Control and U87-FABP7 transfected cells, stable U251-shControl and U251-shFABP7-1 & U251-shFABP7-2 transfected cells, and transient ED501N control and siFABP7-1 and siFABP7-2 transfected cells. (b) Laurdan imaging analysis of membrane lipid order in U87 and U251 stable transfectants, and ED501N transient transfectants. Representative merged pseudo-colored GP images are shown, with color range indicated by the color bar. Purple-red colors (arrows point to plasma membrane) indicate high membrane order and lower fluidity, whereas green-blue colors indicate low membrane order and increased fluidity. Scale bars = 20 μm. (c) Distribution of the GP index values in GBM cells described in a and b. The histograms for U87-FABP7 cells are shifted to the right (higher GP value) compared to U87-Control cells. FABP7-depleted U251 and ED501N cells are shifted to the left (lower GP value). (d) Average GP index values in GBM cells were calculated from several images including the ones shown in panel b (n = 7–10). Statistical analysis of U87 was performed using the two-tailed unpaired t-test. Statistical analysis of U251 and ED501N was performed with one-way ANOVA and Dunnett multiple comparisons test. Center line, median; box limits, 25th and 75th percentiles; whiskers, minimum to maximum with all points shown. ** indicates $p < 0.01$, *** indicates $p < 0.001$, **** indicates $p < 0.0001$, and ns indicates $p > 0.05$. GP, generalized polarization.

GBM neurosphere cells, we observed similar results as with our U87 and U251 cell lines, with ED501N siControl cells showing a higher plasma membrane order compared to FABP7-depleted ED501N cells (both ED501N siFABP7-1 and siFABP7-2) (Fig. 1b–d). These combined results are particularly noteworthy in the context of FABP7 localization to cell protrusions in migratory cells and suggest a link between FABP7-induced ordered plasma membrane and GBM cell migration.

Migratory GBM cells have higher membrane lipid order

A previous study using the Laurdan assay showed an association between cell migration in HeLa cells and membrane lipid order.[32] To address whether this also applies to GBM cells, we used Transwell inserts to separate migratory cells from non-migratory cells using FABP7-expressing U251 and A4-004N cells. Of note, migratory GBM cells have already been shown to express high levels of GBM neural stem cell-like markers compared to their non-migratory counterparts.[34]

Cells (25 000 per well) were seeded in Transwell inserts and allowed to migrate across the porous membrane towards the bottom reservoir containing 10% FCS over a period of 20 hours. After removal of either the non-migratory (retained on top of the membrane) or migratory cells (located at the bottom of the membrane) from duplicate inserts, the remaining cells (bottom membrane representing migratory cells in one case and top membrane representing non-migratory cells in the other case) were stained with the Laurdan dye. Our results indicate that migratory GBM cells have a higher plasma membrane order (higher GP value) compared to non-migratory cells. This was observed for both U251 and A4-004N cells

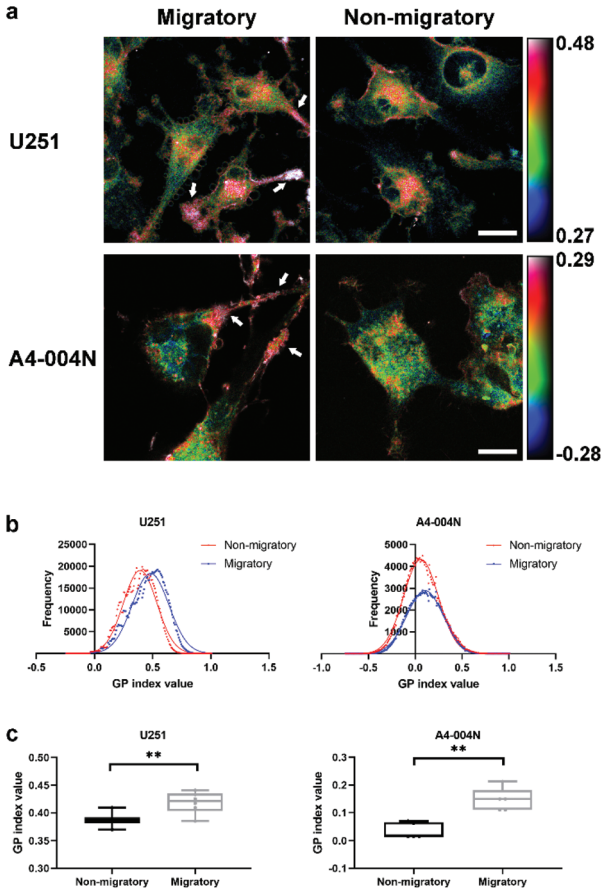

Fig. 2 Migratory GBM cells have a higher membrane order. Laurdan imaging analysis of membrane lipid order in migratory U251 and A4-004N cells (bottom of Transwell inserts) and their non-migratory counterparts (top of Transwell inserts). (a) Representative merged pseudo-colored GP images are shown, with the color range indicated by the color bar. Scale bars = 20 μm. (b) Distribution of GP index values in GBM cells described in panel a. The histograms of migratory U251 and A4-004N cells are shifted to the right (higher GP value), whereas their non-migratory counterparts are shifted to the left (lower GP value). (c) Average GP index values in migratory and non-migratory GBM cells were calculated from several images including the ones shown in panel a (n = 6). Statistical analysis was performed using the two-tailed unpaired t-test. Center line, median; box limits, 25th and 75th percentiles; whiskers, minimum to maximum with all points shown. ** indicates $p < 0.01$. GP, generalized polarization.

(Fig. 2a–c). Increased migration therefore positively correlates with a more rigid and less fluid plasma membrane in FABP7-expressing GBM cells.

DHA decreases membrane lipid order in FABP7-expressing GBM cells

A defining property of membrane liquid-ordered domains is their tight packing of lipids which is usually associated with high levels of tightly-stacking saturated fatty acids and cholesterol.[12] In contrast, fatty acids with multiple double bonds reduce the tight interaction between phospholipid tails, thereby increasing the fluidity of the plasma membrane. Thus, the fatty acid composition of plasma membrane phospholipids can dramatically alter cell membrane order/fluidity as well as membrane-localized growth factor receptor activity and signal transduction.[16]

We have already shown that DHA inhibits GBM migration in a FABP7-dependent manner.[10] Furthermore, DHA is rapidly incorporated into cell membrane phospholipid bilayers in DHA-supplemented cells, thereby disrupting saturated lipids/cholesterol-dependent lipid domains.[35] In light of FABP7's affinity for DHA and likely role in DHA uptake from the extracellular microenvironment, we examined the impact of FABP7 on DHA-mediated changes in membrane lipid order. For these experiments, we used the following pairs of established GBM cell lines: U251-shControl and U251-shFABP7; U87-Control and U87-FABP7. Cells were cultured in 60 μM DHA for 24 hours and stained with the Laurdan dye. DHA supplementation decreased membrane lipid order (*i.e.*, reduced membrane GP index value) in FABP7-expressing GBM cells (U251-shControl and U87-FABP7); however, little effect on lipid order was observed in FABP7-depleted and negative cells (U251-shFABP7-2 and U87-Control) (Fig. 3a–c).

To further document the role of FABP7 in DHA-mediated changes in GBM membrane lipid order, we carried out the Laurdan assay on additional established GBM cell lines (unmanipulated FABP7-expressing U251 and M049; unmanipulated FABP7-negative T98 and A172) as well as patient-derived FABP7-expressing neurosphere cultures (ED501N and A4-004N, both of which naturally express high levels of FABP7). Similar to what was observed in our paired U87 and U251 cell lines, DHA supplementation significantly decreased membrane lipid order (*i.e.*, decreased GP index value) over the entire cell membrane and abolished high-GP regions in all FABP7-expressing GBM cell lines/neurosphere cultures, but had little effect on FABP7-negative GBM cells (Fig. S1a–c†). Thus, our results support a role for FABP7 in increasing the incorporation of DHA in membrane phospholipids, thereby disrupting GBM plasma membrane rigidity and ability to migrate.

Like DHA, AA is a PUFA, but with only four double bonds compared to DHA's six double bonds. As FABP7 can also bind AA, albeit with lesser affinity than DHA, and AA is generally associated with pro-tumorigenic properties, we were particularly interested in whether AA can also alter GBM plasma membrane lipid order. For these experiments, we analysed FABP7-expressing U251 cells cultured in 60 μM AA, compared to BSA control or 60 μM DHA. In contrast to DHA supplementation, AA supplementation had no effect on membrane GP values in GBM cells, generating results similar to BSA control cells (Fig. S2a–c†).

FABP7 localizes to the highly ordered lipid regions of GBM plasma membrane

FABP7 co-localizes with actin at the leading edge of GBM cells cultured in AA-rich medium, suggesting a role for FABP7 in cell migration.[5] Unliganded FABP7 has been shown to directly associate with the plasma membrane.[29,30] Once bound by fatty acids, FABP7 dissociates from the plasma membrane, presum-

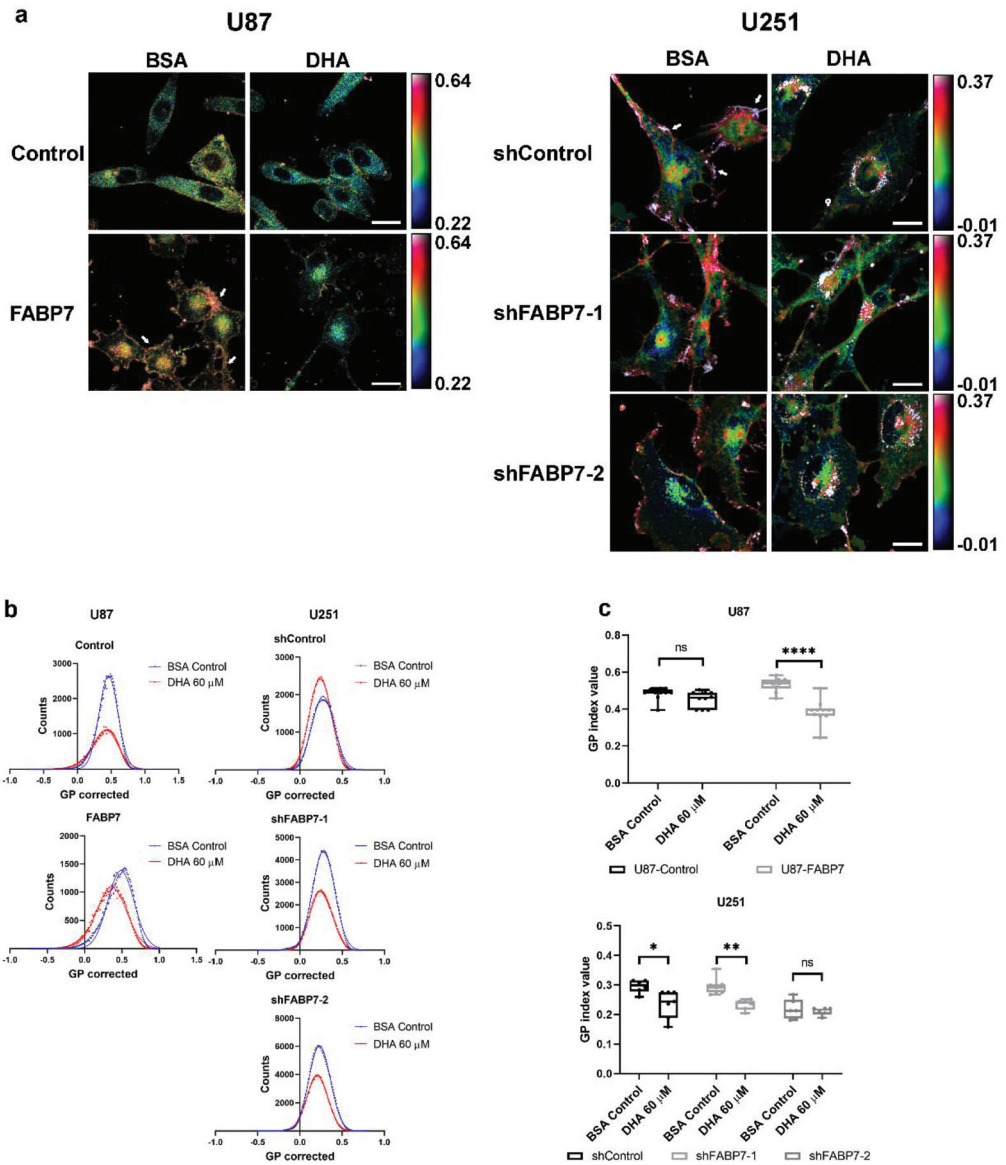

Fig. 3 DHA decreases membrane lipid order in FABP7-expressing GBM cells. (a) Laurdan imaging analysis of membrane lipid order in U87 and U251 stable transfectants (U87-Control & U87-FABP7, U251-shControl & U251-shFABP7) treated with BSA control or 60 μM DHA for 24 hours. Representative merged pseudo-colored GP images are shown, with color range indicated by the color bar. Scale bars = 20 μm. (b) Histograms of FABP7-expressing GBM cells (U87-FABP7 and U251-shControl) are shifted to the left (lower GP value) upon DHA treatment, whereas histograms of FABP7-depleted GBM cells (U87-Control and U251-shFABP7) show no shift upon DHA treatment. (c) Average GP index values were calculated from several images including the ones shown in panel a (n = 6–10). Statistical analysis was performed with multiple t-test using the Holm-Sidak method, with alpha = 0.05. Center line, median; box limits, 25th and 75th percentiles; whiskers, minimum to maximum with all points shown. * indicates $p < 0.05$, ** indicates $p < 0.001$, **** indicates $p < 0.0001$, and ns indicates $p > 0.05$. GP, generalized polarization.

ably to take its cargo inside the cell.[29,30] We therefore used the Texas Red-conjugated Wheat Germ Agglutinin (WGA) membrane marker to investigate whether FABP7 is located at the plasma membrane. Co-staining U251 cells with WGA-Texas Red and anti-FABP7 antibody revealed FABP7 at the leading edge of membrane protrusions (filopodia and lamellipodia; indicated by arrows). As well, FABP7 was observed in the cytoplasm, nucleus and perinuclear region (Fig. 4a).

Actin accumulation at cell membrane protrusions is tightly associated with membrane bound protein distribution, and activation of cytoskeleton remodelling proteins as well as cell signaling pathways.[36] The Laurdan assay has already been used to confirm that cytoskeleton remodelling proteins preferentially localize to highly ordered membrane regions with a high GP value in cancer cells.[32,37] To pursue the relationship between FABP7 located at the leading edge of membrane protrusions and membrane order, we stained U251 cells with anti-FABP7 antibody and the Laurdan dye. Confocal images show that FABP7 accumulates at highly ordered plasma membrane regions (with a high GP values) (Fig. 4b).

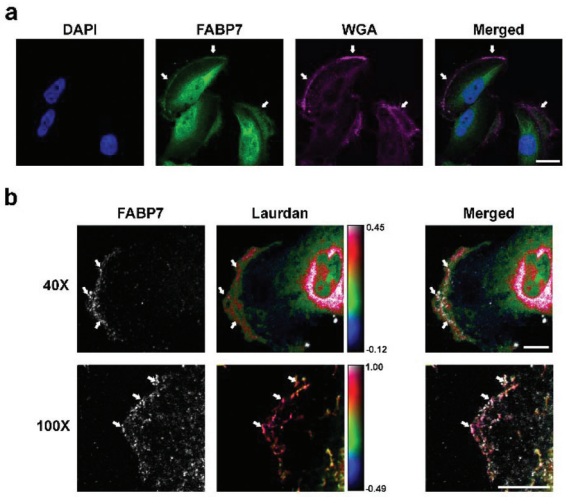

Fig. 4 FABP7 localizes to highly ordered regions of GBM plasma membrane. (a) U251 cells were co-stained with anti-FABP7 antibody (detected with Alexa 488 anti-mouse secondary antibody) and plasma membrane marker WGA-Texas Red. Arrows point to plasma membrane regions. Scale bar = 20 μm. (b) U251 cells were co-stained with anti-FABP7 antibody (detected with Alexa 647 anti-mouse secondary antibody) and Laurdan dye. Images were taken using either a Zeiss confocal microscope (40× oil lens) or a Leica confocal microscope (100× oil lens). Representative merged pseudo-colored GP images are shown for the Laurdan assay. The color range is indicated by the color bar. Arrows point to FABP7 located at highly ordered plasma membrane regions. Scale bars = 10 μm.

FABP7 forms membrane nanoscale domains in GBM cells

Membrane liquid-ordered domains are believed to be nanoscale domains (<200 nm), thus conventional optical microscopy cannot be used to directly investigate nanoscale domain structures because of the limit of its resolution (~250 nm).[12] To overcome this limitation, several super-resolution optical tools have been developed to address membrane lipid-mediated protein nanoscale organization.[18] Using these new tools, actin cytoskeleton protein (*i.e.*, Rac1) has been shown to form nanoscale domains at the plasma membrane in migrating cells.[21,38]

To address the nanoscale distribution of membrane-localized FABP7, we used STED super-resolution microscopy in conjunction with fluorophore-conjugated antibodies which allows a spatial resolution of 30–60 nm with deconvolution. U251 cells were cultured on high-performance coverslips, and immunostained with Atto 550- or Alexa 546-conjugated primary anti-FABP7 antibodies. The localization of FABP7 on the basal surface (closest to the coverslip) of cell membrane protrusions was examined by *Z*-stack scanning (~100 nm stack thickness) with deconvolution. Our results indicate that FABP7 forms nanoscale domains on the plasma membrane in the submicron range (with diameters ranging from 50–150 nm) (Fig. S3†).

DHA disrupts FABP7 nanoscale domain formation in GBM cell membrane

DHA supplementation affects membrane-associated protein organization and downstream signaling pathways based on super-resolution microscopy. For example, DHA has been shown to alter KRas and neurotrophin receptor TrkB nanoscale distribution by re-arranging or disrupting membrane protein nanoscale domains.[25,39] When FABP7 binds to its preferred ligand DHA,[27,28] it undergoes a conformational change that causes it to dissociate from the plasma membrane.[29,30] We were therefore interested in investigating the effect of DHA on the nanoscale domain properties of membrane FABP7, including size, density, inter-domain distance, intensity and shape.

FABP7-expressing U251, ED501N and A4-004N cells were cultured in 60 μM (U251 cells) or 30 μM (ED501N and A4-004N neurosphere cultures) DHA, AA or saturated stearic acid (SA) for 24 hours, with BSA serving as the fatty acid treatment control. Our results revealed reduced FABP7 nanoscale domain formation when the three cell lines were cultured in DHA-supplemented medium compared to BSA-, AA- or SA-supplemented medium (Fig. 5a). The sizes of the majority of FABP7 nanoscale domains ranged from 0.01–0.015 μm^2 (100 nm in diameter) when cells were cultured in their normal (non fatty acid-supplemented) growth medium (DMEM for U251 cells and DMEM/F12/B-27/EGF/FGF neurosphere medium for ED501N and A4-004N). However, upon DHA supplementation, a decrease in membrane FABP7 nanoscale domain size was observed in all three GBM cell lines compared to BSA control. While AA- and SA- supplementation also resulted in a decrease in FABP7 nanodomain size in U251 cells, this decrease was of much lower magnitude compared to that observed with DHA supplementation (Fig. 5b).

In addition to a reduction in size, we observed a significant reduction in the average density of membrane FABP7 nanoscale domains upon DHA supplementation (6-fold decrease in U251 cells, 10-fold decrease in both ED501N and A4-004N) (Fig. 5c). To gain more insight into the spatial distribution of membrane FABP7, we calculated the distance between nearest nanoscale domains using a nearest neighbour distance (NND) analysis algorithm. The overall FABP7 interdomain distance distribution (Fig. S4a†) and the average interdomain distance (Fig. 5d) were significantly increased in DHA-supplemented U251, ED501N and A4-004N cells compared BSA-supplemented cells. Quantitative analyses revealed a >2-fold increase in the average interdomain distance of FABP7 (500–600 nm) upon DHA treatment compared to ~200–250 nm in BSA-supplemented cells (Fig. 5d). Again, the strongest effects were observed in ED501N and A4-004N cultures. Neither AA nor SA supplementation affected the FABP7 interdomain distance of FABP7-expressing U251, ED501N and A4-004N, with the exception of SA-supplementation in U251 cells which increased the FABP7 interdomain distance to ~150 nm (Fig. 5d). Similarly, quantitative analysis of FABP7 nanoscale domain intensity also showed attenuation in all three cell lines upon DHA supplementation compared to BSA control based on immunofluorescence intensity scores (Fig. S4b†). AA and SA supplementation had no effect on FABP7 nanoscale domain intensity.

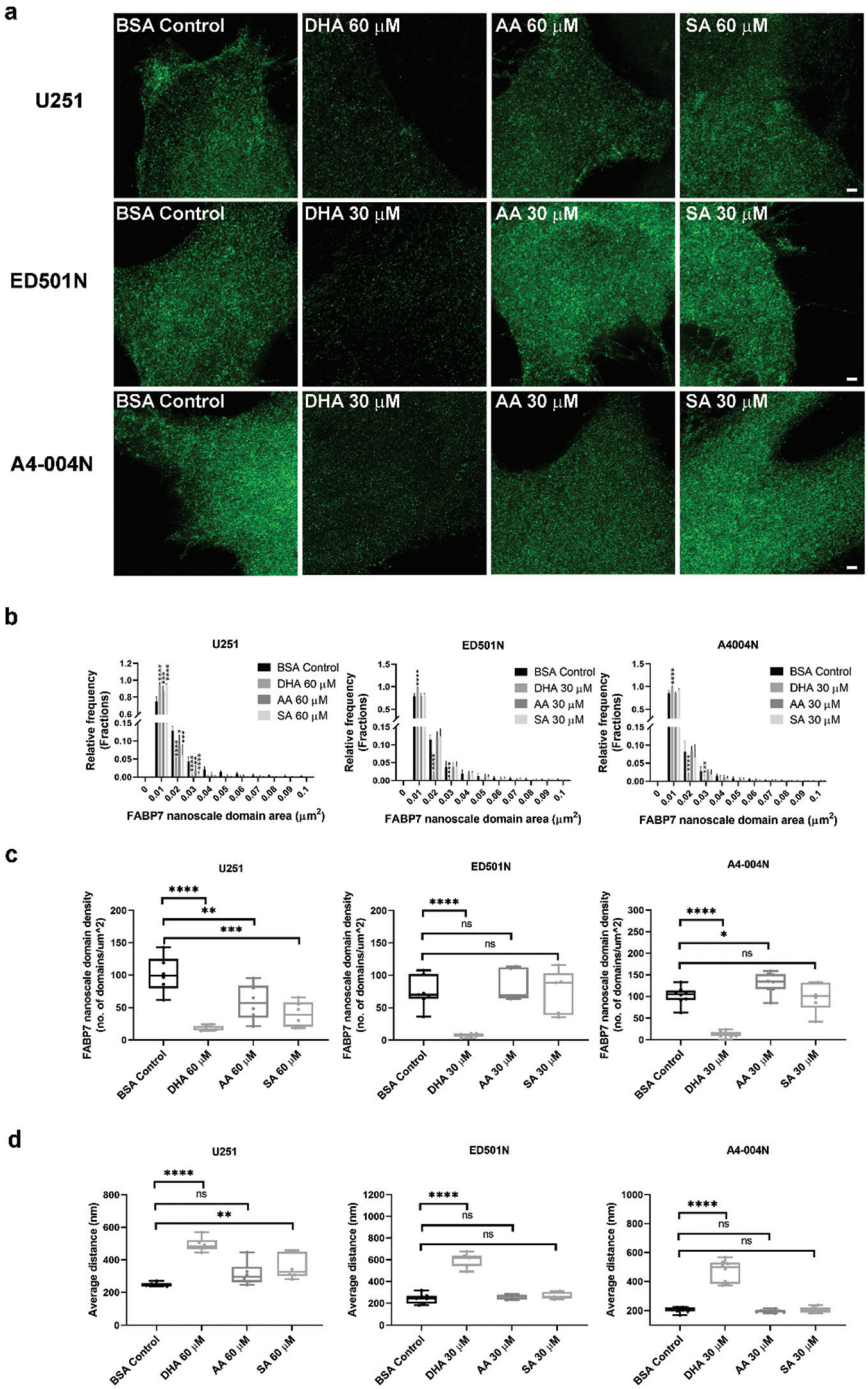

Fig. 5 DHA disrupts FABP7 membrane nanoscale domains in GBM cells. U251, ED501N and A4-004N GBM cells were supplemented with BSA (Control), 60 μM or 30 μM DHA, AA, or SA for 24 hours, then labelled with Atto 550-conjugated primary anti-FABP7 antibody for STED microscopy. Images were taken in *Z*-stack mode and processed using deconvolution. Maximum intensity projections are shown for the different fatty acid treatment conditions. (a) Membrane FABP7 nanoscale domains in GBM cells show reduced density distribution upon DHA treatment compared to BSA control and supplementation with AA or SA. Scale bars = 1 μm. (b) The size distribution of membrane FABP7 nanoscale domains are significantly decreased upon DHA supplementation compared to BSA control, and supplementation with AA or SA ($P < 0.0001$, $n = 6$ to 8 for all three GBM cell lines tested). Statistical analysis was performed with multiple *t*-test using the Holm-Sidak method, with alpha = 0.05. Error bars represent standard deviation. (c) The membrane FABP7 nanoscale domain average density in DHA-supplemented cells is significantly decreased compared to BSA control and supplementation with AA or SA ($P < 0.0001$, $n = 6$ to 8 for all three GBM cell lines tested). Nearest neighbour distance analysis (NND) was performed to determine the distance between a FABP7 nanoscale domain and its five nearest neighbors. (d) DHA supplementation increases the average distance between FABP7 nanodomains compared to BSA control and supplementation with AA or SA ($P < 0.0001$, $n = 6$ to 8 for all three GBM cell lines tested). Statistical analysis of (c) and (d) was performed with one-way ANOVA and Dunnett multiple comparisons test. Center line, median; box limits, 25th and 75th percentiles; whiskers, minimum to maximum with all points shown. * indicates $p < 0.05$, ** indicates $p < 0.01$, *** indicates $p < 0.001$, **** indicates $p < 0.0001$, and ns indicates $p > 0.05$.

Finally, we studied the circularity and solidity of membrane FABP7 nanoscale domains in GBM cells cultured in BSA (control) *versus* DHA supplemented medium. The latter induced a more circular and solid FABP7 membrane distribution pattern compared to control cells. In particular, DHA supplementation increased average FABP7 nanodomain circularity and solidity in ED501N by 7% and 10%, respectively, and in A4-004N cells by 19% and 14%, respectively, compared to BSA control. In comparison, there was no change in circularity and solidity upon AA and SA supplementation in ED501N and A4-004N cells (Fig. S4c and d†). In contrast to neurosphere cultures, DHA, AA and SA supplementation in U251 cells all had effects on the circularity and solidity of FABP7 nanoscale domains, although effects were strongest with DHA supplementation. Regions selected for shape analysis are shown in Fig. S5.† Our results indicate an important role for DHA in the disassembly of FABP7 nanodomains which has broad implications for the regulation of GBM cell migration.

EGFR is a well-characterized protein expressed in GBM cells that forms well-defined membrane nanodomains.[40] We next asked whether other membrane-associated proteins are also affected by DHA supplementation in GBM cells. For this experiment, we cultured U251 cells in serum-free DMEM supplemented with 60 μM DHA for 24 hours. We then immunostained the cells with anti-EGFR antibody. STED microscopy showed that DHA supplementation did not disrupt EGFR nanodomain organization, indicating that not all membrane proteins are susceptible to DHA-mediated disruption of nanodomains (Fig. S6†).

Migratory GBM cells show increased FABP7 membrane nanoscale domain formation

Migrating/motile cancer stem cells define a subgroup of cells with properties associated with a more invasive/metastatic phenotype.[41] Notably, stem cell markers (CD44 and ALDH1) are expressed at elevated levels in the cells located at the leading edges of invasive breast cancer tumors,[42,43] as well as migrating front of breast cancer cells using the *in vitro* scratch assay.[44] Similar to CD44 and ALDH1 in breast cancer, FABP7 can be found at the leading edge of GBM tumors.[5] As our results indicate that FABP7 forms nanoscale domains at the GBM plasma membrane, we next investigated whether there was a correlation between FABP7 membrane distribution and GBM cell migration. U251, ED501N and A4-004N cells were cultured on high performance cover glass and a scratch introduced pre-confluency. Cells were allowed to migrate into the scratch over a period of 24 hours. Cells were then fixed, immunostained with anti-FABP7 antibody and super-resolution STED microscopy carried out at both the migrating front and control areas. STED deconvolution images showed higher expression of FABP7 (right shifting of intensity score curve) at the migrating front compared to control areas for all three GBM cell lines (Fig. S7a†). We also found that migratory GBM cells have a higher density of FABP7 nanodomains which are also larger compared to those observed in non-migrating cells in all three GBM cell lines (Fig. 6a and b). The increase in FABP7 average nanodomain density at migrating fronts ranged from 2.5× for U251 and 5× for ED501N, to 16× for A4-004N (Fig. 6c). Consistent with our density analysis, there was also a significantly decreased inter-domain distance, ranging from ~35–50%, between FABP7 nanodomains in the migrating fronts of all three GBM cell lines based on NND analysis (Fig. 6d and Fig. S7b†). Interestingly, migratory cells also showed less circular FABP7 membrane signals compared to non-migrating cells (~6% and 13% decreases in ED501N and A4-004N cells, respectively), in agreement with highly migratory GBM cells forming more condensed, and thus more irregular FABP7 nanoscale domains at plasma membranes associated with migrating fronts (Fig. S7c and d†).

FABP7 translocates from plasma membrane to mitochondria upon DHA supplementation

Similar to DHA-treated cells, non-migratory GBM cells form fewer FABP7 nanodomains compared to cells cultured in DHA-poor medium. To address whether reduced FABP7 nanodomain formation is the result of reduced overall FABP7 levels or redistribution of FABP7 within the cells, we examined the overall levels of FABP7 in U251, ED501N and A4-004N cells cultured for 24 hours in DHA-supplemented medium. DHA supplementation had no effect on FABP7 protein levels based on western blot analysis of whole cell lysates (Fig. S8a–c†), consistent with our published data in U87-FABP7 cells.[10]

FABPs are lipid chaperones that not only facilitate lipid uptake but transport lipids to different sites within the cell including mitochondria, ER and nucleus.[26] We still have a poor understanding of the role of fatty acid ligands in regulating the subcellular localization of FABPs. When we used confocal microscopy to visualize U251 cells immunostained with anti-FABP7 Atto 550-conjugated primary antibody, we observed a punctate immunostaining pattern throughout the cytoplasm that was reminiscent of mitochondria staining (Fig. S9†). To further address the localization of FABP7 in the cytoplasm of GBM cells, we carried out co-staining analysis of U251, ED501N and A4-004N cells with Atto 550-conjugated primary anti-FABP7 antibody and MitoTracker® Deep Red followed by STED microscopy. As we were particularly interested in the possible localization of FABP7 to the mitochondria, we fixed the cells with glyoxal to maximize the preservation of mitochondria.[45]

Images acquired by dual-color STED microscopy showed FABP7 co-compartmentalization with MitoTracker® Deep Red in all three GBM cell lines (Fig. 7). For quantification analysis, we acquired confocal microscopy images at lower magnification using a 40×/NA1.3 oil lens in order to capture more representative pictures. FABP7 signal was quantified with masks selected by MitoTracker® Deep Red staining pattern in ImageJ (Fig. 8a). We found that FABP7 intensity increased ~1.5 to 2-fold in all three DHA-supplemented GBM cell lines compared to control cells (Fig. 8b). Thus, a preferred site for DHA intracellular transport by FABP7 is mitochondria.

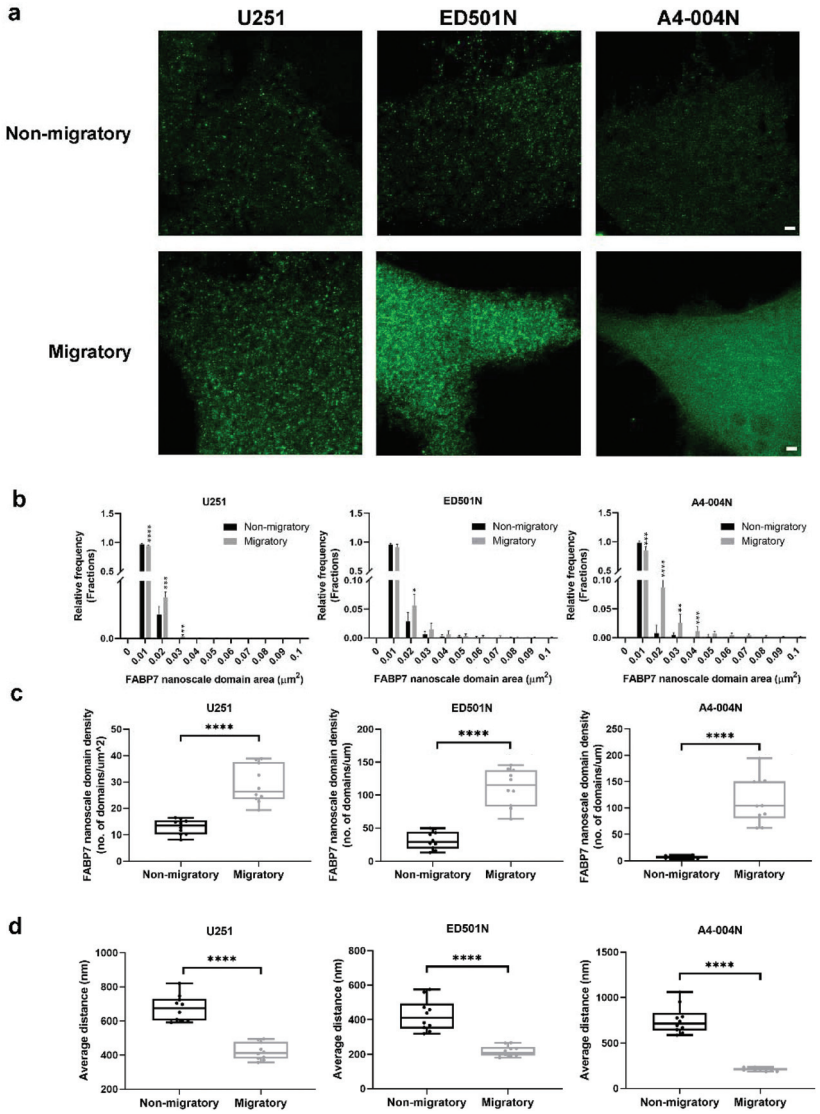

Fig. 6 FABP7 nanoscale domains on GBM membranes are differentially distributed in migratory and non-migratory cells. U251, ED501N and A4-004N were cultured on high-performance coverslips, and the scratch assay carried out to separate GBM migratory cells (migrating fronts) from non-migratory cells (control areas). Cells were then immunostained with Atto 550-conjugated primary anti-FABP7 antibody for STED microscopy. Images were taken in *Z*-stack mode and processed using deconvolution. Maximum intensity projections are shown for migratory cells and non-migratory cells. Scale bars = 1 μm. (a) Membrane FABP7 nanoscale domains in migratory GBM cells show a more condensed distribution compared to cells in control regions. (b) The size of membrane FABP7 nanoscale domains increases in cells located in the migrating front compared to control regions (n = 10 for all three GBM cell lines tested). Statistical analysis was performed with multiple t-test using the Holm-Sidak method, with alpha = 0.05. Error bars represent standard deviation. (c) The membrane FABP7 nanoscale domain average density in migratory cells is significantly increased compared to cells located in control regions ($P < 0.0001$, n = 10 for all three GBM cell lines tested). Nearest neighbour distance analysis (NND) was performed to determine the distance between a FABP7 nanoscale domain and its five nearest neighbors. (d) The average inter-domain distance is decreased in migratory cells compared to cells located in control regions ($P < 0.0001$, n = 10 for all three GBM cell lines tested). Statistical analysis of (c) and (d) was performed with two-tailed unpaired t-test. Center line, median; box limits, 25th and 75th percentiles; whiskers, minimum to maximum with all points shown. ** indicates $p < 0.01$, *** indicates $p < 0.001$, and **** indicates $p < 0.0001$.

Discussion and conclusion

High membrane lipid order and nanoscale domain formation are tightly associated with increased cell migration and infiltrative properties in different cancer types, including GBM.[16,46] Plasma membrane components assemble into well-defined nanoscale domains at the leading edges of cells, with the migrating front exhibiting distinct biophysical properties (*i.e.*, increased membrane rigidity) and cytoskeleton remodelling,[13] key determinants of tumor migratory/infiltrative signalling

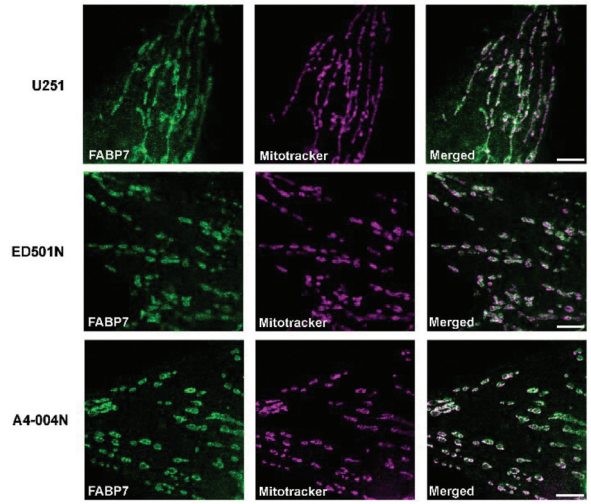

Fig. 7 FABP7 localizes to the mitochondria of GBM cells. Dual-color STED microscopy shows cytoplasmic FABP7 (detected with Atto 550-conjugated primary anti-FABP7 antibody) co-compartmentalizes with mitochondria (MitoTracker® Deep Red) in U251, ED501N and A4-004N cells. Scale bars = 5 μm.

events.[46] FABP7 is an important marker of poor survival in GBM patients[8,47,48] and is preferentially expressed at sites of infiltration in GBM tumors.[5] FABP7 drives cell migration in GBM cells, a property that can be reversed by supplementing the culture medium with DHA.[10] Previously described roles for FABP7 include cytoplasmic lipid droplet formation[49] and activation of nuclear receptors.[9,10] Here, we used a combination of Laurdan assay, FABP7 manipulation and super-resolution microscopy to show that FABP7 expression is associated with increased lipid membrane order, with FABP7 forming nanodomains at the membrane protrusions of GBM cells. By examining migratory *versus* non-migratory cells, we observed a correlation between a highly ordered FABP7 membrane nanoscale assemblies and increased migration in GBM cells. These results were observed in both GBM cell lines and patient-derived GBM cells cultured under conditions that select for neural stem-like cells.

DHA is an exceptionally long (22 carbon chain) and flexible (6 double bonds) fatty acid.[31] Incorporation of DHA in cell membranes can dramatically affect membrane properties, with accompanying effects on membrane protein function.[50] As an example, dietary DHA inhibits oncogenic KRas-driven cell proliferation *in vivo* by rearranging KRas nanoscale domain organization.[25] A striking finding of our study is that DHA supplementation, specifically in FABP7-expressing GBM cells, caused remodelling of membrane lipids to a less ordered state. This membrane lipid remodelling was accompanied by a reduced density of FABP7 nanoscale domains in the plasma membrane and decreased GBM cell migration. These DHA-mediated effects were not observed when cells were cultured in either AA-supplemented or saturated fatty acid-supplemented medium. Furthermore, DHA-supplementation of non-FABP7-expressing GBM cells had no effect on either membrane lipid order or cell migration.

FABP7's preferred ligands are long chain PUFAs, with an ~4× stronger binding affinity for ω-3 PUFA DHA compared to ω-6 PUFA AA.[27,28] DHA is generally linked to anti-tumorigenic properties[51] whereas AA is generally linked to pro-tumorigenic properties.[52] For example, AA supplementation *in vitro* induces Rho-GTPase-mediated cytoskeleton remodelling and cell migration in metastatic human prostate cancer and melanoma cell.[53,54] In GBM cells, AA supplementation *in vitro* induces cyclooxygenase 2 and the formation of prostaglandin E2, promoting cell migration.[10] The brain is a fat-rich tissue with exceptionally high levels of AA and DHA. In adult brain, DHA levels are higher than AA.[55] GBM tissue, on the other hand, has higher levels of AA than DHA.[23] As the availability of AA in GBM tumor tissue may be greater than that of DHA, FABP7 may be primarily bound to AA in these tumors, a condition that may promote cell migration and tumor invasion. It's already known that DHA can be rapidly incorporated into phospholipid bilayers to replace saturated fatty acids and disrupt cholesterol-dependent lipid domains.[35,56] Thus, our results suggest that FABP7, when bound to DHA, induces membrane remodelling properties associated with inhibition of GBM cell migration.

Plasma membranes are composed of a heterogeneous mixture of lipids and proteins, which can be organized to form specific nanoscale domains (10–200 nm), facilitating cellular signaling transduction.[12] In recent years, increased accessibility of super-resolution microscopy has helped to resolve the nanoscale organization of a number of membrane proteins, including EGFR and TrkB.[39,40] Addition of DHA to SH-SY5Y neuroblastoma culture medium caused a significant disruption of TrkB receptor nanoscale clusters on the cell surface. To the best of our knowledge, no one has studied FABP membrane nanoscale distribution to date. Compared to the traditional optical microscope, our STED super-resolution images combined with directly conjugated primary FABP7 antibodies revealed non-uniform distribution of FABP7 on the plasma membrane of GBM cells, with FABP7 localized to highly ordered irregular nanoscale domains <150 nm in diameter. These FABP7 nanoscale domains were most abundant at the basal surface of GBM cell membrane protrusions.

Our results indicate that FABP7 nanodomains have increased size/intensity/domain density and lower circularity/solidity under low-DHA/high-AA culture conditions, suggesting greater FABP7 membrane accumulation as well as coalescing of individual FABP7 nanoscale domains into larger domains, particular in more migratory GBM cells. In GBM cells cultured in DHA-supplemented medium, we observed notably reduced numbers of FABP7 membrane nanodomains as well as reduced membrane FABP7 expression (*i.e.*, decreased intensity and size) and increased membrane FABP7 lateral segregation (*i.e.*, increased inter-domain distance and circularity). These altered properties would likely inhibit any FABP7-dependent GBM migration events. In contrast to FABP7 nanodomains, EGFR nanodomains were not affected by DHA supplementation, indicating a specific role for FABP7 nanodomains in inhibiting cell migration when bound to DHA.

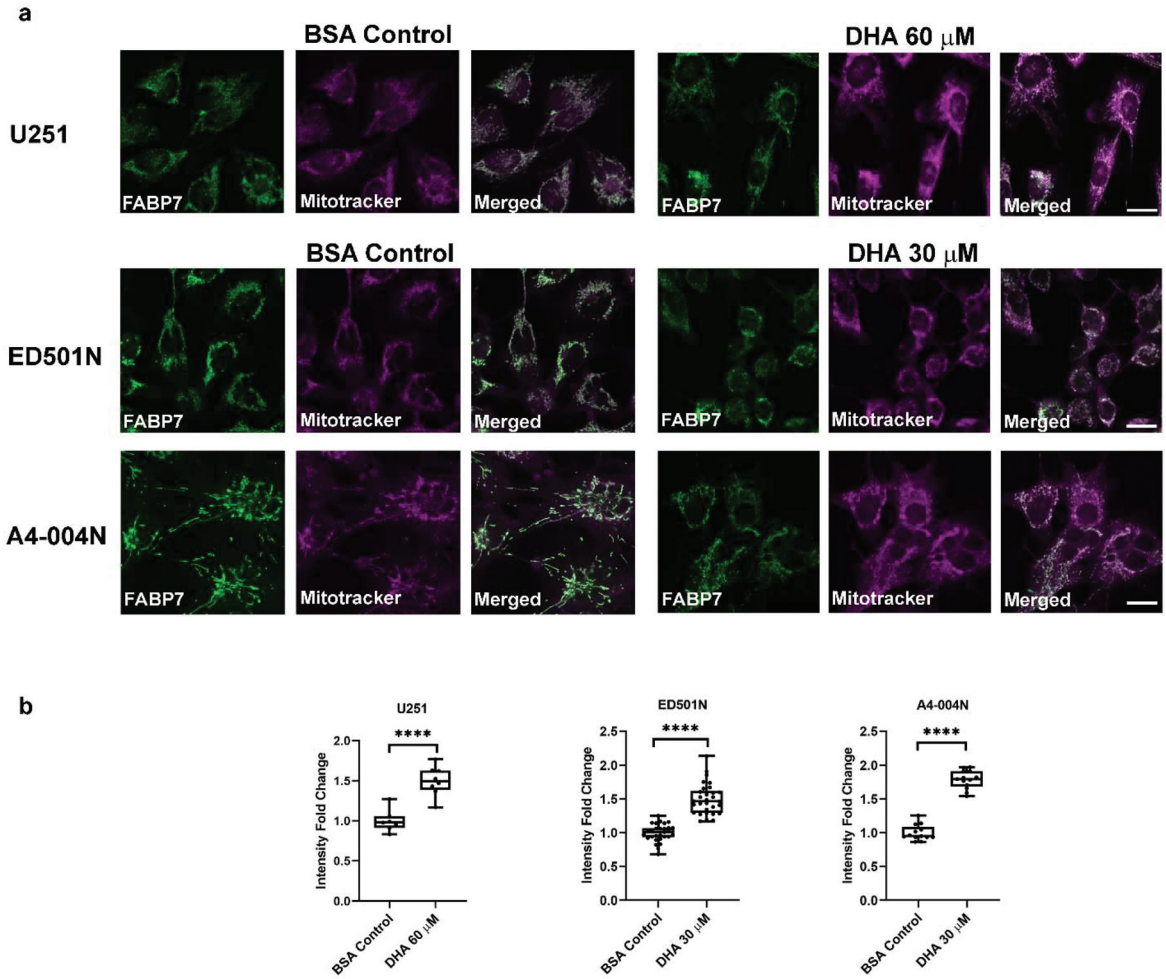

Fig. 8 DHA supplementation relocates FABP7 to mitochondria in GBM cells. (a) Confocal images of FABP7 and MitoTracker® Deep Red co-staining in U251, ED501N and A4-004N cells cultured under BSA Control or DHA 60 μM (U251)/30 μM (ED501N and A4-004N) supplemented conditions. Scale bars = 20 μm. (b) Quantification analysis of mitochondrial FABP7 average intensity in U251 cells, ED501N and A4-004N cells cultured under control (BSA) or DHA 60 μM (U251)/30 μM (ED501N and A4-004N) supplemented conditions. Statistical analysis was performed with two-tailed unpaired *t*-test. Center line, median; box limits, 25th and 75th percentiles; whiskers, minimum to maximum with all points shown. **** indicates $p < 0.0001$.

FABPs not only promote fatty acid/lipid uptake from the microenvironment, but also transport lipids to specific compartments within the cell, such as nucleus, ER and mitochondria.[26] For example, both I-FABP and L-FABP have been shown to transport their fatty acid ligands to mitochondria.[57,58] In support of FABP7 playing a role in mitochondria, FABP7 is expressed at high levels in GBM slow-cycling cells (likely neural stem-like cells) which are characterized by increased mitochondria oxidative phosphorylation.[48] Our data indicate that, like I-FABP and L-FABP, FABP7 also co-compartmentalizes with mitochondria. Intriguingly, growth of GBM cells in DHA-supplemented medium increased the overall intensity of the FABP7 signal localizing to mitochondria. These results are surprising as DHA is not normally recognized as a substrate for fatty acid β-oxidation, although there is evidence from the literature that DHA can localize to the mitochondria. For example, fluorescent-tagged DHA (DHA-BODIPY) localizes to mitochondria in lymphoma cells.[59,60] One possibility is that FABP7 and its fatty acid ligands, and especially DHA, affects mitochondrial function by altering the composition of fatty acids in its membranes. Emerging data from cardiomyocytes and colon cancer cells indicate that DHA incorporates into cardiolipin,[60,61] a mitochondrial-specific phospholipid located at the inner mitochondrial membrane which functions as a platform for anchoring and clustering mitochondrial proteins (*e.g.*, cytochrome C).[62] In some cancer cells, DHA-rich cardiolipin has been shown to alter mitochondrial membrane lipid organization, enhance oxidative stress, and trigger cytochrome-C release and apoptosis.[61,63]

We propose the following model to explain the role of FABP7 in GBM cell migration. When GBM cells are cultured under standard conditions or in AA-supplemented medium, FABP7 forms nanoscale domains at the plasma membrane, promoting membrane lipid order and cell migration. We postulate that FABP7 exists in a primarily unliganded state under these conditions, as liganded FABP7 has previously been

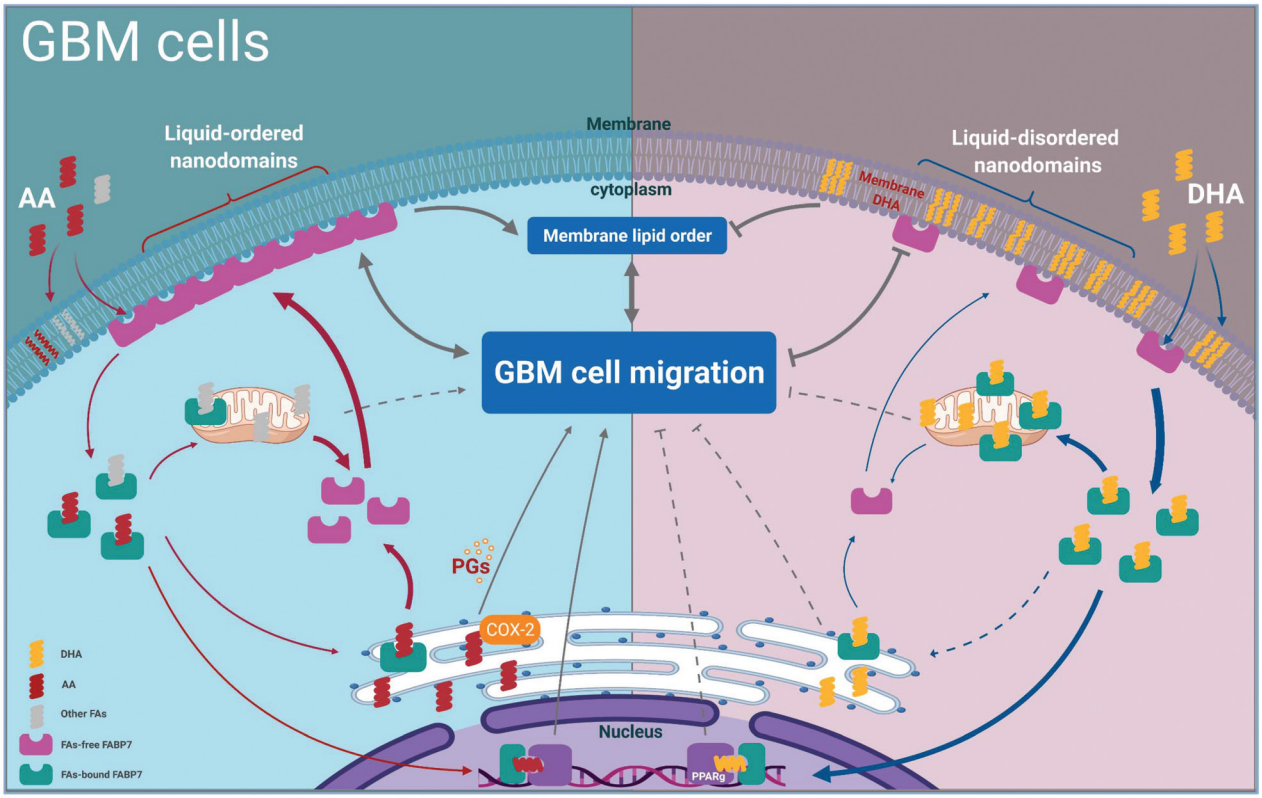

Fig. 9 Schematic model showing the effect of DHA on GBM plasma membrane remodelling and FABP7 distribution. (Left) Under AA-rich culture conditions, FABP7 rapidly cycles between liganded and unliganded states, releasing AA in the cytoplasm for conversion to bioactive metabolites such as prostaglandins (PGs) or fatty acid β-oxidation. Unliganded FABP7 is found in nanoscale liquid-ordered domains, promoting membrane lipid order and cell migration. (Right) Under DHA-rich culture conditions, FABP7 binds to DHA, and liganded FABP7 dissociates from the cell membrane. The high affinity of FABP7 for DHA prevents rapid release of DHA and rapid cycling of FABP7 back to the cell membrane, thereby disrupting FABP7 membrane nanoscale domains, decreasing membrane lipid order and inhibiting GBM cell migration. At least some of the DHA-liganded FABP7 locates to the mitochondria, where it may alter mitochondrial membrane properties. Although not tested here, DHA-liganded FABP7 may also relocate to the nucleus with DHA then activating nuclear factors such as PPARs.

shown to dissociate from biomimetic model membranes.[29,30] When bound to AA, FABP7 may be rapidly recycled back to the plasma membrane after releasing AA in the cytoplasm for conversion to bioactive metabolites such as prostaglandins[10] that promote GBM cell migration and tumorigenic properties (Fig. 9 left). In contrast to AA, when cells are cultured in DHA-supplemented medium, FABP7 nanodomains and cell membrane lipid order are disrupted, and cell migration in inhibited. We propose that recycling of DHA-liganded FABP7 is much slower than that of AA-liganded FABP7 because of FABP7's greater affinity for DHA.[27,28] DHA-bound FABP7 relocates to the mitochondria (shown here) and possibly other structures in the cell such as the nucleus[10] (Fig. 9 right).

In conclusion, we provide evidence that FABP7 expression has a profound effect on the biophysical properties of GBM cell membranes. FABP7's effect on GBM membranes is dependent on the relative levels of its preferred fatty acid ligands in the extracellular microenvironment. Under non-DHA-supplemented growth conditions, FABP7 increases lipid order and formation of nanoscale domains in the plasma membrane of GBM cells, processes accompanied by increased cell migration; however, lipid order, FABP7 nanodomains and cell migration are all disrupted when cells are cultured in DHA-rich medium. These results are observed in both FABP7-expressing established GBM cell lines and in patient-derived GBM neurosphere cultures. Intriguingly, membrane dissociated FABP7 accumulates at mitochondria when GBM cells are cultured in DHA-supplemented medium, suggesting a link between DHA, mitochondria and decreased cell migration. Our findings point to FABP7-dependent lipid remodelling as being a critically important determinant of cell migration in GBM. Based on our results, we postulate that increasing DHA content in the GBM microenvironment is a valid strategy for reducing GBM infiltration in brain.

Materials and methods

Cell lines and transfections

The established human GBM cell lines have been previously described.[10,64] GBM cells (*e.g.*, U251, M049, T98 and A172) were cultured in Dulbecco's modification of Eagle's minimum

essential medium (DMEM) supplemented with 10% fetal calf serum (FCS). Clonal populations of U87 cells stably transfected with pREP4 vector (U87-Control or U87C) or a pREP4-FABP7 expression construct (U87B or U87-FABP7) have previously been described.[5] Patient-derived GBM neurosphere cultures (A4-004N) were prepared by enzymatic and mechanical dissociation of GBM tissues and plating the cells in DMEM/F12 medium supplemented with B-27 (Life Technologies, Carlsbad, CA, USA), epidermal growth factor (EGF), and fibroblast growth factor (FGF). ED501 GBM neurosphere (ED501N) cultures were obtained from Drs. Hua Chen and Kenneth Petruk, University of Alberta. GBM tissues from patients were consented prior to surgery under Health Research Ethics Board of Alberta Cancer Committee Protocol #HREBA CC-14-0070.

Fatty acid preparation and treatment

Fatty acids (DHA and AA) (Sigma) were dissolved in ethanol, then complexed to BSA (Sigma) over a steady stream of nitrogen gas and stored at −80 °C under reducing conditions. Both GBM neurosphere cultures and GBM adherent cells were maintained at 37 °C in a humidified 5% CO_2 atmosphere. For fatty acid supplementation, cells (at 60–70% confluency) were cultured under serum-free conditions and supplemented with BSA (vehicle control), 30 μM or 60 μM DHA, AA, or SA in their regular growth medium (neurosphere medium for A4-004N and ED501N and DMEM for U251) for 24 hours.

shRNA knockdown and siRNA knockdown

Lentivirus shRNA packaging plasmids and control plasmids were purchased from Sigma. The two lentivirus FABP7 shRNA constructs used for our experiments were obtained from the University of Alberta RNAi Core Facility, with the following shRNA sequences: CCGGGAAACTGTAAGTCTGTTGTTACTCGAGTAACAACAGACTTACAGTTTCTTTTTG (shFABP7-1) and CCGGGTGACCAAACCAACGGTAATTCTCGAGAATTACCGTTGGTTTGGTCACTTTTTG (shFABP7-2). Control vector was MISSION pLKO.1 (Sigma-Aldrich, SHC002). For virus production, lentiviral plasmids were transfected into HEK293T cells along with lentivirus packaging vectors (Sigma Mission), and virus-containing supernatant was collected 48 hours after transfection. U251 GBM cells were infected with lentivirus overnight and medium was changed after infection. Infected cells were selected in 1 μg mL^{-1} puromycin. GBM neurosphere cultures (ED501N) were transfected with 10 nM scrambled siRNA (control) or FABP7 siRNAs (5′-CAAACCAACGGUAAUUAUCAGUCAA-3′ (NM_001446 _stealth_405) and 5′-GCUUUCUGUGCUACCUGGAAGCUGA-3′ (NM_001446_stealth_304) (Invitrogen) using LipofectamineTM RNAiMAX (Invitrogen). siRNA-transfected cells used for the Laurdan assay were seeded onto coverslips 48 hours post-transfection.

Western blot analysis

Whole cell lysates were prepared as previously described.[65] Lysates (50 μg per lane) were separated by sodium dodecyl sulfate-polyacrylamide gel electrophoresis (SDS-PAGE) and transferred to nitrocellulose membranes. Membranes were immunoblotted with rabbit anti-FABP7 (prepared in-house; 1:1000)[5] and mouse anti-GAPDH (Thermo Fisher Scientific; 1:1000) antibodies, followed by anti-rabbit or anti-mouse secondary antibodies (Invitrogen, 1:50000).

Quantitative analysis of cell membrane lipid order using Laurdan

Quantification imaging of GBM cell membrane lipid order was carried out using the Laurdan dye (Thermo Fisher Scientific) as described previously.[15] GBM cells were plated on coverslips in 24-well dishes and cultured to ~70% confluency. The Laurdan dye was diluted in serum free DMEM medium to a final concentration of 5 μM. Live cells were washed with 1× PBS and stained with 5 μM Laurdan dye in a humidified incubator (37 °C with 5% CO_2) for 30 minutes. Laurdan-stained cells were then fixed in 4% paraformaldehyde (PFA) for 10 minutes. For co-immunofluorescence of FABP7 and Laurdan dye, fixed cells were labelled with anti-FABP7 antibody (Santa Cruz, 1:400, sc-374588) and anti-mouse Alexa 647 secondary antibody (1:400, Invitrogen).

Images were acquired with a Zeiss LSM 710 confocal microscope (excitation at 405 nm; emission at 400–460 nm for ordered phase imaging and 470–530 nm for disordered phase imaging) with a 40×/1.3 oil-immersion objective as described previously.[15] For co-immunofluorescence of FABP7 and Laurdan dye, a Zeiss confocal 40×/1.3 oil objective and a Leica confocal 100×/1.40 oil objective were used. Liquid-ordered and liquid-disordered phase images were acquired and analyzed using ImageJ software following published guidelines.[15] Merged mean intensity and rainbow RGB pseudo-colored generalized polarization (GP) images are shown. GP values of 8–10 images (total of 30–40 cells analyzed) were quantified from GP images for generation of GP scatter plot histograms using GraphPad Prism 8 software (GraphPad Software, Inc. San Diego, CA, USA). Statistical analyses for the Laurdan assay are presented using the merged mean GP values for each image.

Immunofluorescence assay

For co-immunofluorescence analysis of FABP7 and cell membrane dye wheat germ agglutinin (WGA) Texas Red™, the WGA dye was diluted to 5 μg mL^{-1} using Hank's balanced salt solution (HBSS). GBM cells adhering to coverslips were incubated in WGA dye for 15 minutes at 37 °C. Labelled cells were washed two times with HBSS, then fixed with 4% paraformaldehyde (PFA) for 10 minutes at room temperature, followed by immunostaining with anti-FABP7 antibody (Santa Cruz, 1:400, sc-374588) and anti-mouse Alexa 488 secondary antibody (1:400, Invitrogen).

To enhance the FABP7 cell membrane nanoscale domain immunofluorescence signal for super-resolution microscopy imaging, we used glyoxal to fix cells along with fluorophore-conjugated primary antibody, as described.[45] Cells were cultured on high performance coverslips (D = 0.17 mm ± 0.005 mm, Carl Zeiss) for analysis using the STED microscope. The coverslips were coated with laminin (50 μg mL^{-1}, Sigma-Aldrich) to improve attachment of cells cultured under neuro-

sphere conditions.[66] GBM cells were fixed in 3% glyoxal pH 4 (Sigma-Aldrich) for 30 minutes on ice, followed by 30 minutes at room temperature. Fixation was then quenched with 100 mM NH_4Cl for 20 minutes, and cells were blocked with 2.5% BSA in 1× PBS for 15 minutes. Cells were then incubated with Atto 550-conjugated affinity-purified rabbit primary anti-FABP7 antibody (1:20; conjugation was with the Atto 550 Protein Labeling Kit from Sigma-Aldrich) or Alexa 546-conjugated primary anti-FABP7 antibody (1:20; Santa Cruz, sc-374588) for 60 minutes. For EGFR detection, U251 cells were immunostained with anti-EGFR antibody (Cell signalling, 1:400, #4267) and anti-rabbit Alexa 555 secondary antibody (1:400, Invitrogen). Cells were washed in high-salt PBS (500 mM NaCl), then 1× PBS, and embedded in Prolong Diamond Antifade Mountant (Thermo Fisher Scientific). The cells were imaged using a STED microscope.

For co-staining of FABP7 and mitochondria, live cells were stained with 200 nM MitoTracker® Deep Red FM (Thermo Fisher Scientific) for 30 minutes at 37 °C, followed by 4% PFA or 3% glyoxal pH 4 fixation and quenching with 100 mM NH_4Cl as described.[45] Cells were permeabilized in 2.5% BSA and 0.1% Triton-X 100 in 1× PBS for 15 minutes and labelled with Atto 550-conjugated primary anti-FABP7 antibody (1:100, conjugation was with the Atto 550 Protein Labeling Kit from Sigma-Aldrich) for 60 minutes for dual-color STED microscopy imaging or Zeiss confocal microscopy imaging. For quantitative analysis upon BSA control/DHA treatment, raw images (n = 15, 70–80 cells) were acquired using a Zeiss LSM 710 confocal microscope with a 40×/1.3 oil-immersion objective. The average mitochondrial FABP7 intensity of each image and quantitative analysis were carried out using ImageJ software.

STED microscopy imaging and data analysis

A Leica TCS SP8 Falcon STED microscope was used for our experiments. The inverted microscope was operated with a 100×/1.40 oil objective (HC Plan APO CS2). Quantitative imaging was achieved using Leica HyD detectors HyD 562 nm–648 nm and HyD 660 nm–768 nm. For single-color STED imaging, a laser wavelength of 557 nm was used for excitation of the Atto 550 or Alexa 546-conjugated primary anti-FABP7 antibodies and the depletion laser was set at a wavelength of 660 nm. For dual-color STED imaging (FABP7 co-stained with MitoTracker® Deep Red), MitoTracker® Deep Red images were scanned first (excitation laser wavelength 660 nm, depletion laser wavelength 775 nm), followed by acquisition of FABP7 images with Atto 550-conjugated primary anti-FABP7 antibody (excitation laser wavelength 557 nm, depletion laser wavelength 660 nm). Images with a pixel size set to 23.75 nm were scanned at 100 Hz. For each image data set, a 100 nm Z-stack (at 20 nm intervals) was collected and processed with the LAS X Lightning package for deconvolution to reduce out-of-focus signal and to enhance the signal-to-noise ratio of the final images.

ImageJ software was used for quantitative analysis of FABP7 cell membrane nanoscale domain size, density, intensity, shape, and inter-domain distance. For intensity statistics, maximum intensity projections of the deconvolved images were exported to ImageJ software. Thirty to forty images of 100 pixels × 100 pixels were randomly selected from each image and exported to ImageJ. The pixel intensity of the images had a range of 0–255 (pixel intensity) and the number of pixels at each intensity level was counted. The intensity of each STED image is represented by the average pixel count at each intensity level. Ten images from each of 3 independent experiments were analyzed.

For nanoscale domain size quantification, the maximum intensity projections of the deconvolved images were exported and thresholded for particle analysis. A threshold was established for each cell line based on the most accurate representation of the immunostained images. The threshold established for each cell line was used for all treatment conditions. Images were saved and processed with ImageJ software. The Nearest Neighbour Distance (NND) ImageJ plugin script was used for inter-domain distance calculation.[67] Statistical analyses for inter-domain distance and nanodomain density are presented using the average mean values of each image for comparison. ImageJ particle analyzer was used for nanoscale domain distribution and shape analysis (an area with more than 2 pixel^2 was counted as a particle). Frequencies with different inter-domain distance and size were summarized. Both circularity and solidity of the nanodomains measured with ImageJ particle analyzer are based on differences in nanodomain shape. Circularity is defined as the degree to which the particle is similar to a circle (ranges from 0 to 1, with 1 indicating a perfect circle). Solidity measures overall concavity of a particle (ranges from 0 to 1, with 1 indicating a solid particle with regular boundary). The average particle circularity and solidity values for each image were used for comparison.

Transwell and scratch assays for isolating migratory GBM cells

We used a previously published method to isolate migratory GBM cells.[34] Briefly, GBM cells were trypsinized and counted (Coulter Counter). Twenty-five thousand cells in serum-free DMEM (U251 cells) or in DMEM/F12/B-27/EGF/FGF (A4-004N cells) were seeded in Transwell inserts (pore size: 8 μm; Falcon Cell Culture Inserts) placed in a 24-well plate. Cells were allowed to migrate through the Transwell membrane towards the bottom reservoir containing DMEM or DMEM/F12/B-27/EGF/FGF supplemented with 10% FCS. Cells that remained in the top chamber after 20 hours were considered to be non-migratory, whereas cells that had migrated across the membrane were considered to be migratory. Non-migratory and migratory cells were removed from two different reservoirs, using a Q-tip to discard the migratory and non-migratory cells, respectively. The remaining cells (top chamber in one case and bottom chamber in the other case) were stained with Laurdan dye and fixed with 4% PFA for quantitative membrane lipid order staining as described above. Transwell membranes (top membranes for non-migratory cells and bottom membranes for migratory cells) were released from the inserts using a scalpel. Released membranes were mounted onto glass slides and covered with coverslips for imaging.

The scratch assay[68] was used to study FABP7 plasma membrane nanoscale domain formation in GBM migratory cells *versus* non-migratory cells. Previous work from other labs has shown that cells that migrate away from the scratch margin into the cell-free scratch zones are migratory, whereas cells found farthest from the scratch margins are non-migratory.[69] FABP7 immunofluorescence analysis was carried out using STED microscopy. U251, ED501N and A4-004N cells were cultured on high performance laminin-coated cover glasses (D = 0.17 mm ± 0.005 mm, Carl Zeiss) until they reached 70%–80% confluence. A top-to-bottom scratch was introduced in the middle of the coverslip with a P20 pipet tip, and cells were incubated for an additional 24 hours. Cells were washed with 1× PBS and fixed in glyoxal using the immunostaining method described in above. For FABP7 membrane nanoscale domain analysis, images of cells in the migratory zones and non-migratory zones were collected using a Leica TCS SP8-gated STED microscope. Quantitative data analysis was as described above.

Statistics

Two-tailed unpaired *t*-test was used to assess the significance of differences between two experimental groups. If more than two experimental groups are present in a graph, either multiple *t*-test with Holm-Sidak method (alpha = 0.05) or one-way ANOVA with Dunnett multiple comparisons test was used to evaluate the statistical significance depending on the experimental design. The exact statistical methods used for each experiment is indicated in the figure legends. Prism 8 (GraphPad Software, Inc. San Diego, CA, USA) was used for statistical analysis of data. A *p*-value or adjusted *p*-value of <0.05 was considered significantly different. All experiments were done in triplicate (technical replicates) and were repeated at least three times (biological replicates). All imaging data analysis was based on an average of eight to ten images for each experiment.

Author contributions

X.X., Y.W. and R.G. designed the study; X.X. was involved in all experimental aspects of the study, including tissue culture, fatty acid treatments and confocal/super-resolution microscopy; Y.W. performed direct conjugation of FABP7 antibody, image processing, quantification and statistical analysis; X.S. carried out super-resolution microscopy; W.C. did the western blot analyses; X.X., Y.W. and R.G. wrote the paper. All authors reviewed the paper.

Conflicts of interest

The authors declare no conflict of interest.

Acknowledgements

We gratefully acknowledge the support of Gerry Barron, Dr Guobin Sun and the Cross Cancer Institute Cell Imaging Facility. We are grateful to Dr Hua Chen and Dr Kenneth Petruk for the ED501N GBM cell line. This work was supported by a grant from the Canadian Institutes of Health Research – grant number 130314.

References

1 P. Y. Wen and S. Kesari, *N. Engl. J. Med.*, 2008, **359**, 492–507.
2 A. Vehlow and N. Cordes, *Biochim. Biophys. Acta*, 2013, **1836**, 236–244.
3 A. Kurtz, A. Zimmer, F. Schnutgen, G. Bruning, F. Spener and T. Muller, *Development*, 1994, **120**, 2637–2649.
4 L. Feng, M. E. Hatten and N. Heintz, *Neuron*, 1994, **12**, 895–908.
5 R. Mita, J. E. Coles, D. D. Glubrecht, R. Sung, X. Sun and R. Godbout, *Neoplasia*, 2007, **9**, 734–744.
6 A. De Rosa, S. Pellegatta, M. Rossi, P. Tunici, L. Magnoni, M. C. Speranza, F. Malusa, V. Miragliotta, E. Mori, G. Finocchiaro and A. Bakker, *PLoS One*, 2012, **7**, e52113.
7 Y. Morihiro, Y. Yasumoto, L. K. Vaidyan, H. Sadahiro, T. Uchida, A. Inamura, K. Sharifi, M. Ideguchi, S. Nomura, N. Tokuda, S. Kashiwabara, A. Ishii, E. Ikeda, Y. Owada and M. Suzuki, *Pathol. Int.*, 2013, **63**, 546–553.
8 G. Kaloshi, K. Mokhtari, C. Carpentier, S. Taillibert, J. Lejeune, Y. Marie, J. Y. Delattre, R. Godbout and M. Sanson, *J. Neurooncol.*, 2007, **84**, 245–248.
9 A. Adida and F. Spener, *Biochim. Biophys. Acta*, 2006, **1761**, 172–181.
10 R. Mita, M. J. Beaulieu, C. Field and R. Godbout, *J. Biol. Chem.*, 2010, **285**, 37005–37015.
11 G. van Meer, D. R. Voelker and G. W. Feigenson, *Nat. Rev. Mol. Cell Biol.*, 2008, **9**, 112–124.
12 E. Sezgin, I. Levental, S. Mayor and C. Eggeling, *Nat. Rev. Mol. Cell Biol.*, 2017, **18**, 361–374.
13 J. Gomez-Llobregat, J. Buceta and R. Reigada, *Sci. Rep.*, 2013, **3**, 2608.
14 L. S. Prahl, P. F. Bangasser, L. E. Stopfer, M. Hemmat, F. M. White, S. S. Rosenfeld and D. J. Odde, *Cell Rep.*, 2018, **25**, 2591–2604.
15 D. M. Owen, C. Rentero, A. Magenau, A. Abu-Siniyeh and K. Gaus, *Nat. Protoc.*, 2011, **7**, 24–35.
16 J. Bi, T. A. Ichu, C. Zanca, H. Yang, W. Zhang, Y. Gu, S. Chowdhry, A. Reed, S. Ikegami, K. M. Turner, W. Zhang, G. R. Villa, S. Wu, O. Quehenberger, W. H. Yong, H. I. Kornblum, J. N. Rich, T. F. Cloughesy, W. K. Cavenee, F. B. Furnari, B. F. Cravatt and P. S. Mischel, *Cell Metab.*, 2019, **30**, 525–538.
17 P. Sengupta, T. Jovanovic-Talisman, D. Skoko, M. Renz, S. L. Veatch and J. Lippincott-Schwartz, *Nat. Methods*, 2011, **8**, 969–975.
18 E. Sezgin, *J. Condens. Matter Phys.*, 2017, **29**, 273001.
19 M. Bonny, X. Hui, J. Schweizer, L. Kaestner, A. Zeug, K. Kruse and P. Lipp, *Sci. Rep.*, 2016, **6**, 36028.

20 X. Nan, T. M. Tamguney, E. A. Collisson, L. J. Lin, C. Pitt, J. Galeas, S. Lewis, J. W. Gray, F. McCormick and S. Chu, *Proc. Natl. Acad. Sci. U. S. A.*, 2015, **112**, 7996–8001.
21 A. Remorino, S. De Beco, F. Cayrac, F. Di Federico, G. Cornilleau, A. Gautreau, M. C. Parrini, J. B. Masson, M. Dahan and M. Coppey, *Cell Rep.*, 2017, **21**, 1922–1935.
22 M. F. Garcia-Parajo, A. Cambi, J. A. Torreno-Pina, N. Thompson and K. Jacobson, *J. Cell Sci.*, 2014, **127**, 4995–5005.
23 D. D. Martin, M. E. Robbins, A. A. Spector, B. C. Wen and D. H. Hussey, *Lipids*, 1996, **31**, 1283–1288.
24 M. E. Elsherbiny, M. Emara and R. Godbout, *Prog. Lipid Res.*, 2013, **52**, 562–570.
25 N. R. Fuentes, M. Mlih, R. Barhoumi, Y. Y. Fan, P. Hardin, T. J. Steele, S. Behmer, I. A. Prior, J. Karpac and R. S. Chapkin, *Cancer Res.*, 2018, **78**, 3899–3912.
26 M. Furuhashi and G. S. Hotamisligil, *Nat. Rev. Drug Discovery*, 2008, **7**, 489–503.
27 L. Z. Xu, R. Sanchez, A. Sali and N. Heintz, *J. Biol. Chem.*, 1996, **271**, 24711–24719.
28 G. K. Balendiran, F. Schnutgen, G. Scapin, T. Borchers, N. Xhong, K. Lim, R. Godbout, F. Spener and J. C. Sacchettini, *J. Biol. Chem.*, 2000, **275**, 27045–27054.
29 F. Dyszy, A. P. Pinto, A. P. Araujo and A. J. Costa-Filho, *PLoS One*, 2013, **8**, e60198.
30 Y. Y. Cheng, Y. F. Huang, H. H. Lin, W. W. Chang and P. C. Lyu, *Biochim. Biophys. Acta, Mol. Cell Biol. Lipids*, 2019, **1864**, 158506.
31 W. Stillwell and S. R. Wassall, *Chem. Phys. Lipids*, 2003, **126**, 1–27.
32 J. F. Aranda, N. Reglero-Real, L. Kremer, B. Marcos-Ramiro, A. Ruiz-Saenz, M. Calvo, C. Enrich, I. Correas, J. Millan and M. A. Alonso, *Mol. Biol. Cell*, 2011, **22**, 1252–1262.
33 O. Golfetto, E. Hinde and E. Gratton, *Biophys. J.*, 2013, **104**, 1238–1247.
34 V. Adamski, A. D. Schmitt, C. Fluh, M. Synowitz, K. Hattermann and J. Held-Feindt, *Oncol. Res.*, 2017, **25**, 341–353.
35 S. R. Wassall and W. Stillwell, *Biochim. Biophys. Acta*, 2009, **1788**, 24–32.
36 P. K. Mattila, F. D. Batista and B. Treanor, *J. Cell Biol.*, 2016, **212**, 267–280.
37 G. R. Chichili and W. Rodgers, *Cell. Mol. Life Sci.*, 2009, **66**, 2319–2328.
38 K. N. Maxwell, Y. Zhou and J. F. Hancock, *Mol. Cell. Biol.*, 2018, **38**, e00186-18.
39 B. Angelov and A. Angelova, *Nanoscale*, 2017, **9**, 9797–9804.
40 P. S. Boyd, N. Struve, M. Bach, J. P. Eberle, M. Gote, F. Schock, C. Cremer, M. Kriegs and M. Hausmann, *Nanoscale*, 2016, **8**, 20037–20047.
41 T. Brabletz, A. Jung, S. Spaderna, F. Hlubek and T. Kirchner, *Nat. Rev. Cancer*, 2005, **5**, 744–749.
42 C. Yang, M. Cao, Y. Liu, Y. He, Y. Du, G. Zhang and F. Gao, *Oncogene*, 2019, **38**, 7113–7132.
43 H. Pan, N. Wu, Y. Huang, Q. Li, C. Liu, M. Liang, W. Zhou, X. Liu and S. Wang, *Diagn. Pathol.*, 2015, **10**, 66.
44 A. Saha, S. Shree Padhi, S. Roy and B. Banerjee, *J. Stem Cells*, 2014, **9**, 235–242.
45 K. N. Richter, N. H. Revelo, K. J. Seitz, M. S. Helm, D. Sarkar, R. S. Saleeb, E. D'Este, J. Eberle, E. Wagner, C. Vogl, D. F. Lazaro, F. Richter, J. Coy-Vergara, G. Coceano, E. S. Boyden, R. R. Duncan, S. W. Hell, M. A. Lauterbach, S. E. Lehnart, T. Moser, T. F. Outeiro, P. Rehling, B. Schwappach, I. Testa, B. Zapiec and S. O. Rizzoli, *EMBO J.*, 2018, **37**, 139–159.
46 A. Erazo-Oliveras, N. R. Fuentes, R. C. Wright and R. S. Chapkin, *Cancer Metastasis Rev.*, 2018, **37**, 519–544.
47 Y. Liang, M. Diehn, N. Watson, A. W. Bollen, K. D. Aldape, M. K. Nicholas, K. R. Lamborn, M. S. Berger, D. Botstein, P. O. Brown and M. A. Israel, *Proc. Natl. Acad. Sci. U. S. A.*, 2005, **102**, 5814–5819.
48 L. B. Hoang-Minh, F. A. Siebzehnrubl, C. Yang, S. Suzuki-Hatano, K. Dajac, T. Loche, N. Andrews, M. Schmoll Massari, J. Patel, K. Amin, A. Vuong, A. Jimenez-Pascual, P. Kubilis, T. J. Garrett, C. Moneypenny, C. A. Pacak, J. Huang, E. J. Sayour, D. A. Mitchell, M. R. Sarkisian, B. A. Reynolds and L. P. Deleyrolle, *EMBO J.*, 2018, **37**, e98772.
49 K. Bensaad, E. Favaro, C. A. Lewis, B. Peck, S. Lord, J. M. Collins, K. E. Pinnick, S. Wigfield, F. M. Buffa, J. L. Li, Q. Zhang, M. J. O. Wakelam, F. Karpe, A. Schulze and A. L. Harris, *Cell Rep.*, 2014, **9**, 349–365.
50 N. R. Fuentes, E. Kim, Y. Y. Fan and R. S. Chapkin, *Mol. Aspects Med.*, 2018, **64**, 79–91.
51 S. C. Larsson, M. Kumlin, M. Ingelman-Sundberg and A. Wolk, *Am. J. Clin. Nutr.*, 2004, **79**, 935–945.
52 M. Azrad, C. Turgeon and W. Demark-Wahnefried, *Front. Oncol.*, 2013, **3**, 224.
53 M. Brown, J. A. Roulson, C. A. Hart, T. Tawadros and N. W. Clarke, *Br. J. Cancer*, 2014, **110**, 2099–2108.
54 M. C. Garcia, D. M. Ray, B. Lackford, M. Rubino, K. Olden and J. D. Roberts, *J. Biol. Chem.*, 2009, **284**, 20936–20945.
55 Y. Owada, *Tohoku J. Exp. Med.*, 2008, **214**, 213–220.
56 W. Stillwell, S. R. Shaikh, M. Zerouga, R. Siddiqui and S. R. Wassall, *Reprod., Nutr., Dev.*, 2005, **45**, 559–579.
57 P. D. Schley, D. N. Brindley and C. J. Field, *J. Nutr.*, 2007, **137**, 548–553.
58 J. Karsenty, O. Helal, P. L. de la Porte, P. Beauclair-Deprez, C. Martin-Elyazidi, R. Planells, J. Storch and M. Gastaldi, *Mol. Cell. Biochem.*, 2009, **326**, 97–104.
59 H. Teague, R. Ross, M. Harris, D. C. Mitchell and S. R. Shaikh, *J. Nutr. Biochem.*, 2013, **24**, 188–195.
60 S. Raza Shaikh and D. A. Brown, *Prostaglandins Leukot. Essent. Fatty Acids*, 2013, **88**, 21–25.
61 J. Hofmanova, J. Slavik, P. Ovesna, Z. Tylichova, J. Vondracek, N. Strakova, A. H. Vaculova, M. Ciganek, A. Kozubik, L. Knopfova, J. Smarda and M. Machala, *Eur. J. Nutr.*, 2017, **56**, 1493–1508.
62 J. Dudek, *Front. Cell Dev. Biol.*, 2017, **5**, 90.
63 Y. Ng, R. Barhoumi, R. B. Tjalkens, Y. Y. Fan, S. Kolar, N. Wang, J. R. Lupton and R. S. Chapkin, *Carcinogenesis*, 2005, **26**, 1914–1921.

64 M. Brun, S. Jain, E. A. Monckton and R. Godbout, *Neoplasia*, 2018, **20**, 1023–1037.
65 R. Z. Liu, W. S. Choi, S. Jain, D. Dinakaran, X. Xu, W. H. Han, X. H. Yang, D. D. Glubrecht, R. B. Moore, H. Lemieux and R. Godbout, *Mol. Oncol.*, 2020, **14**, 3100–3120.
66 M. Rahman, K. Reyner, L. Deleyrolle, S. Millette, H. Azari, B. W. Day, B. W. Stringer, A. W. Boyd, T. G. Johns, V. Blot, R. Duggal and B. A. Reynolds, *Anat. Cell Biol.*, 2015, **48**, 25–35.
67 Y. Mao, Nearest Neighbor Distances Calculation with ImageJ, https://icme.hpc.msstate.edu/mediawiki/index.php/Nearest_Neighbor_Distances_Calculation_with_ImageJ, (accessed 15, Dec, 2020).
68 C. C. Liang, A. Y. Park and J. L. Guan, *Nat. Protoc.*, 2007, **2**, 329–333.
69 C. Yang, R. R. Iyer, A. C. Yu, R. L. Yong, D. M. Park, R. J. Weil, B. Ikejiri, R. O. Brady, R. R. Lonser and Z. Zhuang, *Proc. Natl. Acad. Sci. U. S. A.*, 2012, **109**, 6963–6968.